A case study on lightning protection, building resonances considered

The transmission cross section $\langle \sigma_{2,1} \rangle$ is determined in (3) from the value of the coupling loss rate coefficient $\Lambda_{2,1}$. This transmission cross section is valid for both strong and weak couplings between the cavities. In the specific case of a well-defined electrically large aperture with physical area *A*, the geometrical optics approximation can be applied to establish [10]

$$\langle \sigma_{2,1} \rangle \cong A/2. \tag{12}$$

The small cavity used in this experiment has a circular (12.7-cm diameter) open aperture on its top wall. Equation (12) is valid if the diameter is greater than approximately a half wavelength. At 4.5 GHz, a half wavelength is 3.3 cm. Substitution of the 12.7-cm diameter value into (12) and (3) yields a calculated value for the coupling coefficient of $\Lambda_{2,1} = 9.5 \times 10^5\ \mathrm{m}^3/\mathrm{s}$. This calculated value compares favorably with the value $\Lambda_{2,1} = 8.9 \times 10^5\ \mathrm{m}^3/\mathrm{s}$ given in (11) from measurements and the model overlay in Fig. 3. The difference in power leakage (4) between these two values of $\Lambda_{2,1}$ is less than 0.3 dB, which is well within measurement uncertainty.

The model solutions for $u_1^\delta(t)$ and $u_2^\delta(t)$ expressed in (6) are the impulse responses for a δ-function excitation that delivers U_0 total energy at time $t = 0\,\mathrm{s}$. As such, they can be used as Green's function kernels in the solution for any time-dependent driving function of power *p*(*t*) injected into a cavity

$$u_1(t) = \int_0^t \frac{u_1^\delta(t-t')}{U_0} p(t')dt'$$
$$u_2(t) = \int_0^t \frac{u_2^\delta(t-t')}{U_0} p(t')dt'. \tag{13}$$

The energy loss rate coefficients are fundamental parameters describing the basic interactions—leakage and ohmic loss—that the reverberant fields undergo. These coefficients are independent of excitation. Two excitations that are common in electromagnetic interference/electromagnetic compatibility testing are the unit step and square pulse functions. For these two simple excitations of power *p*(*t*), the integrals in (13) can be evaluated analytically. For step input, the asymptotic behaviors of $u_1(t)$ and $u_2(t)$ to their steady-state CW values are obtained.

Nested chamber measurements are commonly used for SE studies of enclosures, [11]. SE of an enclosure is often defined in terms of the ratio of steady-state CW energy or power densities inside and outside the test structure

$$\mathrm{SE}^{\mathrm{encl}}(\mathrm{dB}) \equiv -10\log\left(\frac{u_2}{u_1}\right) = -10\log\left(\frac{\Lambda_{2,1}}{\Lambda_2 + \Lambda_{2,1}}\right). \tag{14}$$

For the small nested chamber serving as the test enclosure, the SE calculated from (14) using the energy loss rate coefficients in (11) gives $\mathrm{SE}^{\mathrm{encl}}(\mathrm{dB}) \simeq 6.2\,\mathrm{dB}$.

IV. Conclusion

A time-dependent model of the growth, decay, and exchange of RF energy between coupled complex cavities is presented. The model equations can be solved easily for any level (weak or strong) of coupling between cavities. Hence, cavity couplings originating from many different physical mechanisms, such as window materials, open apertures, closed and open hatches, seams, and cable/pipe penetrations through bulkheads, are accommodated. The time-domain measurements and modeling approach of this paper are particularly well suited for assessing energy propagation and shielding effects in below-deck compartments and passageways in ships, aircraft cabins and bays, and buildings such as hangars and metal storage facilities.

References

[1] G. Tait, M. Hatfield, B. Bernard, and M. Rodriguez, "Electromagnetic complex cavity characterization of a fighter aircraft main weapons bay," in *Proc. IEEE Int. Symp. Electromagn. Compat.*, TX, Aug. 2009, pp. 208–213.

[2] D. A. Hill, *Electromagnetic Fields in Cavities: Deterministic and Statistical Theories*. New York: Wiley-IEEE Press, 2009, ch. 2, 7.

[3] G. B. Tait, R. E. Richardson, M. B. Slocum, M. O. Hatfield, and M. J. Rodriguez, "Reverberant microwave propagation in coupled complex cavities," *IEEE Trans. Electromagn. Compat.*, vol. 53, no. 1, pp. 229–232, Feb. 2011.

[4] G. Tait, M. Slocum, and R. Richardson, "On multipath propagation in electrically-large reflective spaces," *IEEE Antennas Wireless Propag. Lett.*, vol. 8, pp. 232–235, 2009.

[5] R. Richardson, "Reverberant microwave propagation," Naval Surface Warfare Center, Dahlgren Division, Dahlgren, VA, Tech. Rep. NSWCDD/TR-08/127, Oct. 2008.

[6] A. Khaleghi, "Time-domain measurement of antenna efficiency in reverberation chamber," *IEEE Trans. Electromagn. Compat.*, vol. 57, no. 3, pp. 817–821, Mar. 2009.

[7] A. H. Davis, "Reverberation equations for two adjacent rooms connected by an incompletely soundproof partition," *Philos. Mag.*, vol. 50, no. 295, pp. 75–80, Jul. 1925.

[8] A. D. Pierce, *Acoustics: An Introduction to Its Physical Principles and Applications*. New York: McGraw-Hill, 1981, ch. 6.

[9] E. K. Dunens and R. F. Lambert, "Impulsive sound response statistics in a reverberant enclosure," *J. Acoustical Soc. Amer.*, vol. 6, no. 6, pp. 1524–1532, Jun. 1977.

[10] D. A. Hill, M. T. Ma, A. R. Ondrejka, B. F. Riddle, M. L. Crawford, and R. T. Johnk, "Aperture excitation of electrically large, lossy cavities," *IEEE Trans. Electromagn. Compat.*, vol. 36, no. 3, pp. 169–178, Aug. 1994.

[11] *IEC 61000-4-21: Electromagnetic compatibility (EMC): Part. 4-21: Testing and measurements techniques—Reverberation chamber test methods, International Electrotechnical Commission, Geneva, Switzerland, 2008, Annex G, H.*

A Case Study on Lightning Protection, Building Resonances Considered

Alexander P. J. van Deursen and Geesje Bargboer

***Abstract*—In a recent paper (G. Bargboer and A. P. J. van Deursen, *IEEE Trans. Electromagn. Compat.*, vol. 52, no. 3, pp. 684–90, Aug. 2010) we dealt with current injection measurements to test the lightning protection system of a newly built pharmaceutical plant. In a tentative extrapolation, the measurements were extrapolated to actual lightning. Here, we extend the model and calculate the response of the installation on lightning currents and include resonances in the cable trays and test cables contained in it. It turned out that suspension rods between roof support and cable tray were indispensable to suppress the resonances. The time dependence of the present results and the earlier simplified model given in differ greatly, but the amplitudes of induced voltages appear to be of the same order of magnitude.**

***Index Terms*—Industrial plant, lightning protection, modeling, resonance.**

Manuscript received January 18, 2011; revised June 2, 2011; accepted June 4, 2011. Date of publication July 12, 2011; date of current version August 18, 2011. The work was supported by the Dutch Ministry of Economic Affairs of the Innovation Oriented Research Program Electromagnetic Power Technology under Project IOP-EMVT2301A.

The authors are with the Department of Electrical Engineering, Eindhoven University of Technology, Eindhoven, 5600 MB, The Netherlands (e-mail: a.p.j.v.deursen@tue.nl; g.bargboer@tue.nl).

Color versions of one or more of the figures in this paper are available online at http://ieeexplore.ieee.org.

Digital Object Identifier 10.1109/TEMC.2011.2159269

I. Introduction

In the previous report, we presented current injection measurements on a newly built pharmaceutical plant that aim to verify the lightning protection scheme adopted [1], [2]. The measurements agreed with a simplified model of the building, based on the method of moments (MoM) [3], [4]. In this short paper, we extend the model to include resonances in the structure and cables, as is appropriate for faster subsequent strokes.

The building model consisted of three levels (see Fig. 1): the lightning protection grid on the flat roof at 19 m, the steel skeleton to carry the roof at 18.5 m, and the cable support system in the fourth (top) floor, at 3 m below the roof. Downconductors and steel structures brought the lightning current to a system of grounding electrodes in the soil. In the measurements, the injected current was a damped sinusoid of 18 kHz, equivalent to a rise time of 9 μs. The roof skeleton carried 80% of the injected current, and the lightning protection grid carried the remaining 20%. This was also found in the MoM model. The cable support branch 1 (see Fig. 2) carried 1.1%. The model predicted 3%, lowered to 1.7%, if a nearby large diameter airduct was also taken into account as a conductor.

Resonances over the 69-m wide building and support were not measured and, therefore, not considered in [1]. In an extrapolation to actual lightning, this is acceptable for the first stroke with a 10–90% rise time of 8 μs according to the lightning current waveshape proposed in [5]. However, the subsequent stroke rises 40 times faster (0.2 μs) and will excite resonances. Four coupled resonators are, then, relevant for the analysis: 1) the building structure, 2) the support, 3) the cables inside the support, and 4) the cables interior. The half-wavelength resonance in the building occurs at 0.6 MHz and at about 2.0 MHz in the support. As will be shown in Section III, the suspension rods between the cable support and the steel skeleton shift the support resonances to much higher frequencies, where lightning is less important.

II. Model

Several models exist for the distribution of the lightning current over the channel length [6], [7]. The distribution is certainly relevant for the electric fields and induced current of nearby or far-away lightning. For a direct stroke on the building, the current at the point of impact is more important than the channel current at distances larger than the building size. The lightning channel is then modeled as a 200-m long vertical path, excited by a voltage source 1 m above the roof (see Fig. 1). In order to suppress resonances over the lightning path, series impedances were embedded following a profile proposed by Wu and King [8]. In the MoM model, all currents and voltages in the building are, then, related to the current at the base of the source. An upper frequency of 10 MHz suffices. The damping of the resonances is mostly due to the surface impedance of the conductors and to a minor part by reradiation at higher frequencies. The support conductors were modeled with the skin effect. For steel conductors, we included the magnetic property (relative permeability $\mu_r = 200$). In order to estimate the effect of saturation, we repeated the calculation with $\mu_r = 1$ also for steel. With a step of 1 kHz, the density of frequency points is sufficient to describe the resonance damping accurately.

Fig. 2, an adapted copy of Fig. 1(c) in [1], shows the layout of the cable support. In the MoM, three parallel tubes are assumed at positions approximating those of the actual beams [see Fig 2(b)]. In a separate 2-D-MoM calculation, we determined the self-inductance matrix of the actual beams with respect to a wide cylinder surrounding the three beams, and the tube diameters were selected to best fit this matrix. The tube ends are connected to the local downconductors; at the junction of branches 1, 2, and 3, the tubes are interconnected. We consider a bundle

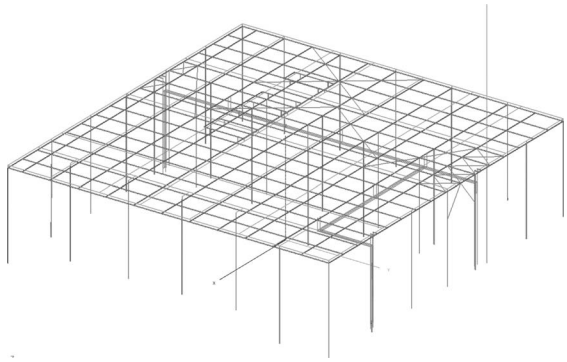

Fig. 1. Model of the $69 \times 71 \times 19$ m^3 pharmaceutical plant. The vertical line at the right extending above the structure indicates the 200-m tall lightning channel. The conduit system inside runs over the full width of the plant.

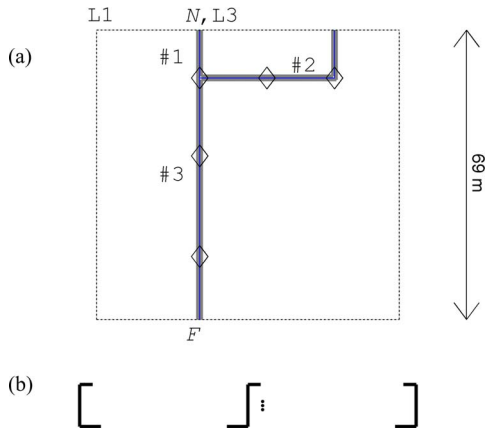

Fig. 2. (a) Support branches routing in the horizontal plane, and the various points and markers are discussed in the text. (b) Support cross section (100 times enlarged), where the three dots indicate the cable positions at 35 mm from the central beam.

of three test cables on the support [1]: 1) a three-lead power cable; 2) a twin-lead power cable with steel armor; and 3) a twin-lead fieldbus cable with its shield consisting of an aluminum foil and a thin copper braid. The cables follow a similar traject as in the actual installation. Fig. 2(b) shows the cable positions with respect to the central beam at the horizontal distance x of 35 mm. See also Fig. 3 in [1]. The cables extend downward over 2 m at the near end (N) close to L3 and 13 m at the far end (F) of Section III. Their total length is 82 m.

The coupling between the MoM-derived support current I_s and the cable leads and shields is described by a mutual inductance M that depends on the position of the cables. The contribution of the support surface impedance is negligible compared to ωM (ω is the angular frequency). The propagation of the transmission line (TL) modes between the cables and the support and those inside the cables is described by the BLT method [9], or rather by the equivalent method presented in [10]. We implemented the distributed coupling via M in a similar way as in [14, Ch. 3] and [15, Ch. 7], extended to multiconductor TLs. The inductance and the capacitance matrix for the cable shields, inner leads, and support result from a quasi-static 2-D calculation [11], where the three interconnected support beams act as common return. The capacitance matrix uses the known dielectric constants of the insulator materials. The cable capacitances and inductances agree with those measured for 1–3-m long cable samples to within 10%. We employ analytical approximations for off-diagonal matrix elements and

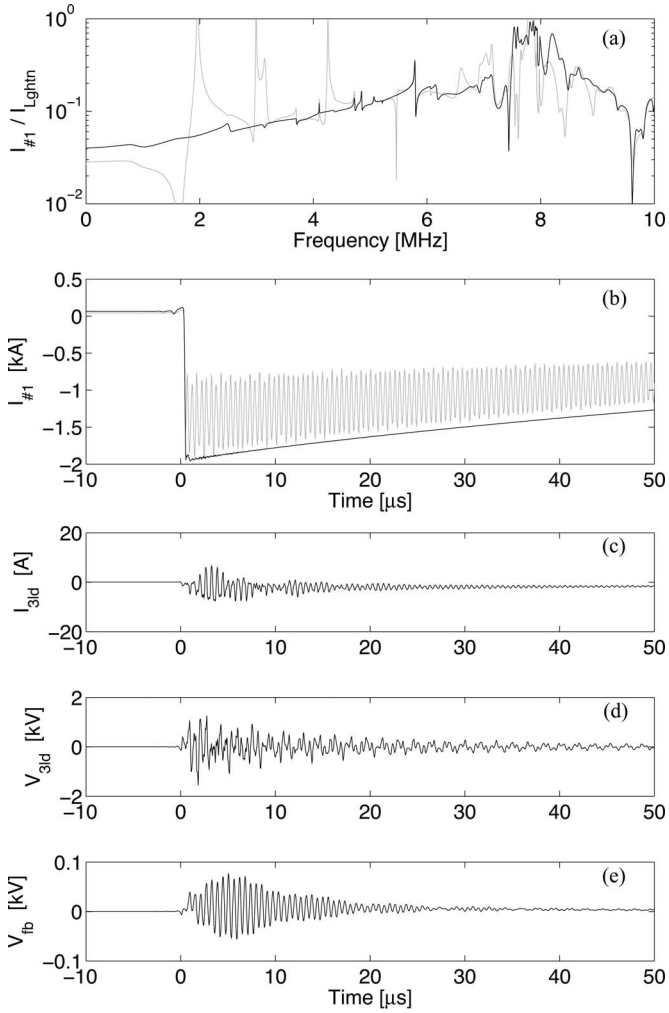

Fig. 3. (a) Transfer between source and support branch 1 near the junction (see Fig. 2) for the case without (gray) and with (black) additional interconnections. (b) Solid line: current in support. (c) and (d) Current and voltage for three-lead cable at the near end with the cable bundle at 35 mm from the central beam. (e) Voltage for the fieldbus cable. Data in (b) up to (e) assume a subsequent stroke at L3 (see Fig. 2).

for the (inner and outer) surface impedances, except for the transfer impedances Z_t.

The measured Z_t of the cable shield or armor has been shown in [1, Fig. 5]. As the Z_t of the shielded or armored cable does not show an increase linear with frequency, even at the highest frequencies near 20 MHz, the skin effect on the wires in the aluminum foil, braid, or armor dominates over the magnetic coupling through the holes in the braid. We conclude that it is also justified to neglect the capacitive coupling Y_t compared to the skin effect Z_t. As in [1], we use the analytical approximation with Bessel functions, describing $|Z_t|$ within a factor of 2 and the phase within 10°.

For shielded cables, the natural mode currents flow in the inner loop (differential mode: inner conductor and inside of shield as return) and the outer loop (common mode: outside of shield and support as return) [12]. The TL formulation in [10] uses the net current through each conductor. The transformation of currents, voltage, and impedance and admittance matrices between the two descriptions has earlier been presented in [13].

TABLE I
PARAMETERS FOR IEC CLASS I LIGHTNING CURRENT

	I [kA]	k	τ_1 [μs]	f_1 [kHz]	τ_2 [μs]	f_2 [kHz]
first	200	0.93	19	50	485	0.33
subseq.	50	0.993	0.454	$2 \cdot 10^3$	143	1.1

We choose two lightning strike positions, L1 at the corner of the building and L3 at about 1 m toward L1, near the conduit end N (see Fig. 2). The calculation starts with the determination of the distribution of the current I_s as sum over the three support tubes for the frequencies 1 kHz up to 10 MHz. In the MoM software FEKO, the maximum length of the elements is 1.5 m and the total number is about 3000. In a postprocessing step, the distributed M-coupling to the TLs is calculated. P and Q integrals [14, eq. 3.4] are determined as a sum over the elements, with the series distributed voltage source $E_z = j\omega M \cdot I_s$. In the TL model, all cables conductors are short circuited to the support at the far end F in Fig. 2, where far is regarded from the lightning attachment point. This was also the case in the experiments [1]. At the near end N, the shield, the ground lead, and the armor are again shorted to the support. For each frequency, we determined the transfer between the source current at one hand and the cable currents to the support near N and F plus the voltage between the open-ended leads and support at N on the other hand. As a final step, the lightning current is considered. We assume the IEC model [5] with the highest severity Class I. The time dependence of the lightning current is

$$i(t) = \frac{I}{k} \times \frac{(t/\tau_1)^{10}}{1 + (t/\tau_1)^{10}} \exp(-t/\tau_2) \tag{1}$$

with parameters given in Table I. The spectrum of $i(t)$ is constant below the frequencies f_2, rolls off $\propto 1/f$ until f_1, where the decay becomes much steeper. The fourier transform of $i(t)$ is multiplied by the transfer functions mentioned earlier to give the response spectra. The response spectra are complex conjugated and mirrored with respect to the maximum frequency of 10 MHz to facilitate fast-fourier transform. We interpolate the spectra into a mesh with 50 Hz steps, to allow a large time domain. The inverse fourier transform, then, provides the time-dependent currents and voltages near end N.

III. RESULT

The results for a lightning stroke at a sensitive point, the top of the conduit system (L3 in Fig. 2), are presented first. We discuss the results for a stroke at the building corner L1 later.

In an introductory calculation, the support and the steel skeleton were only interconnected at the support ends, thus forming an extended resonator with a large quality factor. The gray line in Fig. 3(a) shows the resulting current transfer from source to support branch 1 close to the junction. The first resonance occurred at 1.96 MHz. The oscillatory gray line in Fig. 3(b) represents the corresponding branch 1 current, in the case of excitation by a -50 kA subsequent stroke at L3. In the actual installation, the support is suspended from the skeleton by a large number of rods irregularly spaced at about 2-m distance. The electrical contact between rods, skeleton, and support is present but is not guaranteed. We choose to model this situation by five rods ["$\diamond$" in Fig. 2(a)], which shifted the first resonance upward to frequencies, where the lightning current contributes less. The black line in Fig. 3(a) shows the current transfer between source and support branch 1 for this situation. Below 1 MHz, the transfer is approximately 0.04 and constant. At these frequencies, the current distribution in the building is governed by induction [1, Sect. I]. The transfer rises approximately proportional to the frequency above 1.6 MHz; some resonances are

TABLE II
CABLE CURRENT AND VOLTAGE CALCULATED FOR THE FIRST (F, PEAK CURRENT AND VOLTAGE) AND SUBSEQUENT (S, HALF OF PEAK TO PEAK VALUES) LIGHTNING STROKE, ATTACHED AT POINT L3 OR L1 [SEE FIG 2(a)]

Pos. att.	F/S	3-lead I [A]	3-lead V [kV]	armored I [A]	armored V [kV]	fieldbus I [A]	fieldbus V [kV]
35	F (p)	8	0.07	14	0.03	19	0.04
L3	S (p-p)/2	7	1.4	11	1.4	13	0.07
200	F (p)	23	0.16	28	0.05	43	0.09
L3	S (p-p)/2	17	2.7	21	2.2	31	0.16
35	F (p)	3	0.02	4	0.01	6	0.01
L1	S (p-p)/2	6	0.8	8	0.6	9	0.04
35	S*(p-p)/2	24	3.7	41	3.2	40	0.13

The last line (S*) shows the data omitting the suspension rods in the model.

present. For the 200 kA first stroke at L3, 4% of the current flows through branch 1, in reasonable agreement with the 2.5% mentioned in [1]. The support current has the same waveshape as the lightning current, since the whole building has a dominant inductive behavior below 1 MHz. The smooth black line in Fig. 3(b) shows the response to a -50 kA subsequent stroke. It exhibits only minor oscillations on this scale.

In the support of the actual installation, the cable position varied (see Fig. 3 in [1]). We, therefore, compare two extreme positions: 35 mm, from the central beam, and 200 mm, which is midway between the central and right beam. M varied by a factor of 3, 23, and 69 nH/m, respectively. The cable currents and voltages varied by a factor of 3 or less because of the accompanying change in TL matrices. In the case of a first stroke, the cable currents resemble the lightning current waveshape, but differentiated because of the $j\omega M$ coupling between support and cables. Therefore, we only give the peak values in Table II. The cable currents are less than assumed in [1], mostly since the current through branch 3 of the support is less than one-half of the current through branch 1, and 84% of the cable runs over branch 3. As a result, the voltages are also less than those in [1, Table IV].

In the case of a subsequent stroke, current and voltage for the three-lead cable are shown in Fig. 3(c) and (d). Since the oscillating behavior is dominant, we present half of the peak-to-peak values in Table II. The fieldbus cable behaves similarly, with adapted amplitudes for current and voltage [see Fig. 3(e)], as does the common-mode current through the armored cable. However, the large damping by the armor causes the differential-mode voltage to decay much faster to within less than 10 μs.

We tested the saturation effect, by assuming a relative permeability μ_r of 1 for the steel support. The changes with respect to $\mu_r = 200$ were negligible.

The effect of a power line filter with an assumed 2-nF input capacitor has also been considered. For the subsequent stroke, the voltages on the three-lead and armored cables are reduced by a factor of 2 and 6, respectively. The cable common-mode currents are not affected. For the first stroke, there is only a small reduction, if any at all.

When the current is injected at the point L1 instead of at L3 (see Fig. 2), the support current pattern completely changes. Cable currents and voltages decrease with a factor varying between 4 and 2.5 for both first and subsequent strokes, see Table II.

The last row of Table II gives the values for the cable current and voltages when the cable support is allowed to form a resonating structure with the roof skeleton. Current and voltages are more than a factor of 2, too high in this model.

IV. DISCUSSION

The lightning current waveform has two roll-off frequencies mentioned in Table I. The mutual inductance coupling $\omega M'$ between support and cables rises with frequency. This cable current remains limited by the self-inductance L' of the cable inside the support. The roll-off is counteracted by the increase of the transfer to the support current with frequency, at least up to 8 MHz, see Fig. 3(a). But when the cable length becomes comparable to a quarter wavelength, averaging over the cable length sets in and further increase of the cable current is halted. Z_t of the three-lead cable rises with ω above a few kilohertz, the one for the armored cable rises with $\omega^{1/2}$ above 4 kHz, as does the one for the fieldbus above 200 kHz. The large voltages for the three-lead cable and the armored cable are caused by the increasing Z_t rather than by the larger common-mode currents. All internal cables circuits are open at one end; the odd harmonics of the first quarter wavelength resonances of the armored and fieldbus cables are clearly less pronounced in Fig. 3(c)–(e).

It is interesting to compare the results with the simple model summarized in [1, Table IV], where resonances were neglected. The cable currents of the model presented here are smaller than the values assumed in [1]. As a result, the voltages for the three-lead cable are smaller by a factor of about 5. The same holds for the armored cable, but only in the case of the first stroke. For the subsequent stroke, the voltages are larger than those from the simple model of [1]. This is tentatively attributed to the rise of $|Z_t(\omega)|$, but remains an item for further investigations. The voltages on the fieldbus cable are comparable or a factor of 2 larger.

We used the IEC level I lightning current waveshape, whereas for the building modeled level III with half the amplitudes was requested.

Several assumptions other than those mentioned earlier have implicitly been made in the analysis. We neglected pigtails at the points, where the cable leave the support toward the equipment. Similarly, all other cables on the support (see [1, Fig. 3]) have not been considered, because of lack of information about their paths and common-mode currents. Also, the influence of other conductors on the support current has not been taken into account. As shown in [1], the nearby airduct reduced the support current by a factor of 1.7. The twist of the leads in the cables has not been considered in the calculations. However, twisting would not reduce the coupling between the unbalanced cables and the support current. This is particularly true for the three-lead cable.

V. CONCLUSION

The benefit of a continuous and interconnected cable support is clearly demonstrated by the present lightning-protection model. Many distributed short circuits between support and skeleton suppress low-frequency resonances and improve the lightning protection. Calculated currents do not damage the cables thermally [1]; the voltages are in a range that passive-filter components can handle.

ACKNOWLEDGMENT

The authors recall with gratitude the late Prof. C. E. Baum, who always freely gave advice at meetings and conferences. He suggested to have a better look at the resonances. The authors would like to thank Prof. A. G. Tijhuis for the stimulating discussions.

REFERENCES

[1] G. Bargboer and A. P. J. van Deursen, "A case study of lightning protection, current injection measurements, and model," *IEEE Trans. Electromagn. Compat.*, vol. 52, no. 3, pp. 684–690, Aug. 2010.

[2] G. Bargboer, "Measurements and modeling of EMC, applied to cabling and wiring," Ph.D. dissertation, Dept. Electr. Eng., Eindhoven Univ. Technol., Eindhoven, the Netherlands, May 2011.
[3] *FEKO Users's Manual*, FEKO, Stellenbosch, South Africa, 2008, 2011.
[4] (2010). [Online]. Available: http://www.feko.info
[5] IEC 62305, *Protection Against Lightning*, Geneva: International Electrotechnical Commission, 2006.
[6] Y. Baba and V. A. Rakov, "Applications of electromagnetic models of the lightning return stroke," *IEEE Trans. Power Del.*, vol. 23, no. 2, pp. 800–811, Apr. 2008.
[7] Y. Baba and V. A. Rakov, "Electric and magnetic fields predicted by lightning return stroke electromagnetic models," in *Proc. 20th Int. Zurich Symp. Electromagn. Compat.*, 2009,, pp. 117–120.
[8] T. T. Wu and R. W. P. King, "The cylindrical antenna with nonreflecting resistive loading," *IEEE Trans. Antennas Propag.*, vol. 13, no. 3, pp. 369–373, May 1965 (*ibidem* L. Shen, R. King, pp. 998–998).
[9] C. Baum, T. Liú, and F. Tesche, "On the analysis of general multiconductor transmission-line networks," Albuquerque: Airforce Research Laboratory, Interaction Note 350, Nov. 1978. At present: University of New Mexico.
[10] A. R. Djordjevic and T. K. Sarkar, "Analysis of time response of lossy multiconductor transmission line networks," *IEEE Trans. Microw. Theory Tech.*, vol. MTT-35, no. 10, pp. 898–908, Oct. 1987.
[11] A. van Deursen, F. van Horck, and J. van der Merwe, "A self-optimizing discretization scheme for 2-D boundary element calculations," *J. Electromagn. Waves Appl.*, vol. 15, no. 4, pp. 461–476, 2001.
[12] M. J. A. M. van Helvoort, A. P. J. van Deursen, and P. C. T. van der Laan, "The transfer impedance of cables with a nearby return conductor and a noncentral inner conductor," *IEEE Trans. Electromagn. Compat.* vol. 37, no. 2, pp. 301–306, May 1995.
[13] B. Demoulin and A. P. J. van Deursen, "Deux approches pour établir le lien entre la notion usuelle d'impédance de transfert et le formalisme des lignes couplées," in *Proc. 10èm Colloq. Int. Exposition sur la Compatibilité Electromagn.*, Clermont-Ferrand, France, Mar. 14–16, 2000, pp. 98–103.
[14] E. F. Vance, *Coupling to Shielded Cables*. New York: Wiley, 1978.
[15] F. M. Tesche, M. V. Ianoz, and T. Karlsson, *EMC Analysis Methods and Computational Models*, 2nd ed. New York: Wiley, 1997.

Harmonization of a Bandpass Shielding Enclosure and Its Internal Antenna

Cheng-Nan Chiu and Kuan-Chih Huang

***Abstract*—This paper investigates the way to harmonize a bandpass shielding enclosure (BPSE) and its internal antenna for achieving better performance. The harmonization greatly depends on the relative position of the antenna with respective to the adjacent periodic elements and the sideboards of the BPSE. For this harmonization, an internal high-permittivity dielectric resonator antenna is suggested due to its compact size and the minimum distance allowed between the antenna and the metallic sideboards of the BPSE. In addition, an appropriate zone for locating the antenna is suggested in terms of the relative position between the antenna and its adjacent BPSE elements. According to these suggestions, the antenna can be placed deep within a BPSE corner, a position which is often required in practice.**

***Index Terms*—Frequency-selective surface, shielding, wireless communications.**

Manuscript received January 7, 2011; revised March 20, 2011; accepted March 29, 2011. Date of publication June 30, 2011; date of current version August 18, 2011. This work was supported by the National Science Council of Taiwan under Grant NSC 99-2221-E-212-002.

The authors are with the Department of Electrical Engineering, Da-Yeh University, Changhua 515, Taiwan (e-mail: cnchiu@mail.dyu.edu.tw; skij80233@yahoo.com.tw).

Digital Object Identifier 10.1109/TEMC.2011.2141142

I. Introduction

Modern wireless communication devices, such as mobile phones, personal digital assistants, global positioning systems, and laptop/tablet computers, may use internal antennas mounted on their circuit boards to transmit and receive wireless signals. To ensure electromagnetic compatibility, these devices also need a conductive enclosure to shield the radiated emissions generated from their own digital and RF circuits as well as the radiated noise in their ambiance. At the same time, the enclosure should not affect the radiation performance of the internal antenna. To satisfy such a requirement, a bandpass shielding enclosure (BPSE) has been proposed [1]–[3].

A BPSE is an airtight metallic box with each face (or only the top/bottom faces) designed as a bandpass frequency-selective surface [4]–[8], which has also been applied as an electromagnetic bandgap structure for the suppression of ground bounce noise and radiated emissions in high-speed circuits [9], [10]. A BPSE should allow the transmission of wireless signals transmitted/received by the internal antenna while simultaneously prohibiting the penetration of internal radiated emissions and ambient radiated noise. Consequently, a BPSE should provide high transmittance at a specified wireless signal band and high shielding effectiveness outside this band. In addition, it should not have much influence on the radiation performance of the internal antenna located inside this BPSE. In previous works [1]–[3], typical dipole and loop antennas were considered as the internal antenna. Even though the dipole and loop antennas are representative of the high- and low-impedance radiated sources, respectively, they are too large to be used in practice. In addition, their radiation performance is highly degraded as they are located near the metallic sideboards of the BPSE due to the image current induced on these sideboards.

In this paper, the way to harmonize a BPSE and its internal antenna for better performance is thoroughly investigated. For this harmonization, a high-permittivity dielectric resonator antenna is suggested as the internal antenna. The BPSE-related performance of this antenna is very different from the typical dipole and loop antennas considered in [1]–[3] and from other kinds of metallic antennas. This antenna is not only compact in size but also can be located very near or even directly on the metallic sideboards of the BPSE. The latter benefit results from a newly revealed and applied effect for reducing the image current induced on the neighboring metallic sideboards. For illustration, the internal antenna and BPSE prototypes were created and studied. Based on the results obtained, an appropriate zone for locating the antenna is suggested in terms of the relative position between the internal antenna and its adjacent periodic elements of the BPSE. The results also demonstrate that the internal antenna can be successfully located in the BPSE corners and next to the metallic sideboards without degrading its radiation performance.

II. BPSE and Its Internal Antenna

To demonstrate and investigate the harmonization of a BPSE and its internal antenna, the BPSE and antenna prototypes were designed and created. The BPSE has an IEEE 802.11 b/g/n passband (2400–2484 MHz) and the antenna has the same impedance matching band determined by a 10-dB return loss. As illustrated in Fig. 1(a), the BPSE is an airtight rectangular metallic box that is fully etched with periodic elements on its top and bottom faces. The etched element here is a cross-slot with end loading [see Fig. 1(b)], which is most suitable for the BPSE application [1]. The internal antenna is a dielectric resonator antenna [see Fig. 1(c)] with a ceramic substrate resonator having a high dielectric constant of 80. In Fig. 1(c), the black area indicates the printed metal on the resonator. The reason why the dielectric resonator antenna is highly recommended for this application will be thoroughly